

# $\Lambda$ K femtoscopy in Pb–Pb collisions at $\sqrt{s_{\text{NN}}} = 2.76$ TeV measured with ALICE

Jesse T. Buxton<sup>1</sup> on behalf of the ALICE Collaboration

The Ohio State University, Columbus OH 43210, USA,  
`jesse.thomas.buxton@cern.ch`

**Abstract.** The first measurements of the scattering parameters of  $\Lambda$ K pairs in all three charge combinations ( $\Lambda K^+$ ,  $\Lambda K^-$ , and  $\Lambda K_S^0$ ) are presented. The results are achieved through a femtoscopic analysis of  $\Lambda$ K correlations in Pb–Pb collisions at  $\sqrt{s_{\text{NN}}} = 2.76$  TeV recorded by ALICE at the LHC. The femtoscopic correlations result from strong final-state interactions, and are fit with a parametrization allowing for both the characterization of the pair emission source and the measurement of the scattering parameters for the particle pairs.

**Keywords:** femtoscopy, heavy-ion collisions

## 1 Introduction

Femtoscopy is an experimental method used to study the space–time characteristics of the particle emitting sources in relativistic particle collisions. With this method, two- (or many-) particle relative-momentum correlation functions are used to connect the final-state momentum distributions to the space–time distributions of particle emission at freeze-out [1]. The correlation functions are sensitive to quantum statistics, as well as strong and Coulomb final-state interactions (FSI). Thus, femtoscopy can offer a unique environment in which to measure nuclear scattering parameters, many of which are difficult, if not impossible, to measure otherwise.

## 2 Data analysis

This work reports on the analysis of Pb–Pb collisions at  $\sqrt{s_{\text{NN}}} = 2.76$  TeV produced by the LHC and measured by the ALICE experiment in 2011. Charged particle tracking was performed using the Time Projection Chamber (TPC) and the Inner Tracking System (ITS). Particle identification for reconstructed tracks was carried out using both the TPC and Time-Of-Flight (TOF) detectors in the pseudorapidity range  $|\eta| < 0.8$ . The purities of the  $K^\pm$  collections are estimated to be  $P_{K^\pm} \approx 97\%$  in the range  $0.14 < p_T < 1.5$  GeV/ $c$ . Electrically neutral  $\Lambda$  ( $\bar{\Lambda}$ ) and  $K_S^0$  particles were reconstructed through their weak decays:  $\Lambda \rightarrow p\pi^-$  and  $K_S^0 \rightarrow \pi^+\pi^-$ . The  $\Lambda$  and  $\bar{\Lambda}$  purities are estimated to be  $P_{\Lambda(\bar{\Lambda})} \approx 95\%$  ( $p_T > 0.4$  GeV/ $c$ ), and that of the  $K_S^0$  is  $P_{K_S^0} \approx 98\%$  ( $p_T > 0.2$  GeV/ $c$ ). When

forming particle pairs, a shared daughter restriction is applied to ensure the first particle in the pair is unique from the second. Furthermore, an average separation constraint is imposed to remove splitting and merging effects.

### 3 Analysis methods

The two-particle correlation function is defined as the ratio of the covariant two-particle and single-particle spectra. In practice, the correlation function is formed experimentally as  $C(k^*) = \mathcal{N} \frac{A(k^*)}{B(k^*)}$ , where  $A(k^*)$  is the signal distribution,  $B(k^*)$  is the reference distribution, and  $\mathcal{N}$  is a normalization parameter. The signal distribution is the same-event distribution of particle pairs, and the reference distribution is obtained using mixed-event pairs [2], i.e., particles from a given event are paired with those from another event.

Theoretically, the  $\Lambda K$  correlation function can be described analytically with a model derived by Lednický and Lyuboshitz [3],

$$C(k^*)_{\text{Lednický}} = 1 + \sum_S \rho_S \left[ \frac{1}{2} \left| \frac{f^S(k^*)}{R_{\text{inv}}} \right|^2 \left( 1 - \frac{d_0^S}{2\sqrt{\pi}R_{\text{inv}}} \right) + \frac{2\Re f^S(k^*)}{\sqrt{\pi}R_{\text{inv}}} F_1(2k^*R_{\text{inv}}) - \frac{\Im f^S(k^*)}{R_{\text{inv}}} F_2(2k^*R_{\text{inv}}) \right], \quad (1)$$

where  $f(k^*)$  is the complex scattering amplitude,  $F_1$  and  $F_2$  are analytic functions, and  $R_{\text{inv}}$  is the radius of the spherically symmetric Gaussian distribution assumed for the pair emission source in the pair rest frame. The complex scattering amplitude is evaluated via the effective range approximation,  $f(k^*) = \left( \frac{1}{f_0} + \frac{1}{2}d_0k^{*2} - ik^* \right)^{-1}$ , where  $f_0$  is the complex s-wave scattering length and  $d_0$  is the effective range of the interaction.

*Residual correlations* The finally measured correlation function is a combination of the genuine  $\Lambda K$  correlation with contributions from both impurities and residual correlations resulting from resonance feed-down [4],

$$C_{\text{measured}}(k_{\Lambda K}^*) = 1 + \lambda'_{\Lambda K} [C_{\Lambda K}(k_{\Lambda K}^*) - 1] + \sum_{ij} \lambda'_{ij} [C_{ij}(k_{\Lambda K}^*) - 1], \quad (2)$$

where  $\lambda'_{ij} = \lambda_{\text{Fit}} \lambda_{ij}$ , the  $\Lambda K$  term represents the genuine  $\Lambda K$  correlation, and the  $ij$  terms denote the contributions from impurities and residual correlations. The  $\lambda_{ij}$  parameters serve as weights dictating the relative strength of each component's contribution to the observed signal, and are estimated using the THERMINATOR 2 and HIJING simulations [4, 5]. The net correlation signal from the small subset of pairs containing an impurity (i.e., pairs with at least one misidentified member) is assumed to average to unity. The main sources of residual correlations in the  $\Lambda K$  systems result from  $\Lambda$  hyperons which have decayed from  $\Sigma^0$ ,  $\Xi^0$ , and  $\Xi^-$  parents. When modeling the  $\Sigma^0 K$  and  $\Xi^0 K$  systems, for

which the interactions are not known, the source radii and scattering parameters are assumed equal to those of the daughter  $\Lambda K$  system. For modeling the  $\Xi^- K^\pm$  contribution, the available experimental  $\Xi^- K^\pm$  data are used. Each residual component,  $C_{ij}(k_{\Lambda K}^*)$  in Eq. 2, is the parent correlation function expressed in terms of the relative momentum of the daughter  $\Lambda K$  pair, and is obtained using a transform matrix generated with the THERMINATOR 2 [6] simulation (see [4] for more details).

*Non-femtoscopic background* A significant non-femtoscopic background is observed in all studied  $\Lambda K$  correlations, which is primarily due to particle collimation associated with elliptic flow, and results from mixing events with unlike event planes [7]. Each background is modeled using a 6<sup>th</sup>-order polynomial fit to the THERMINATOR 2 simulation, as shown in Fig. 1, which is then applied as a scale factor in the final fit function.

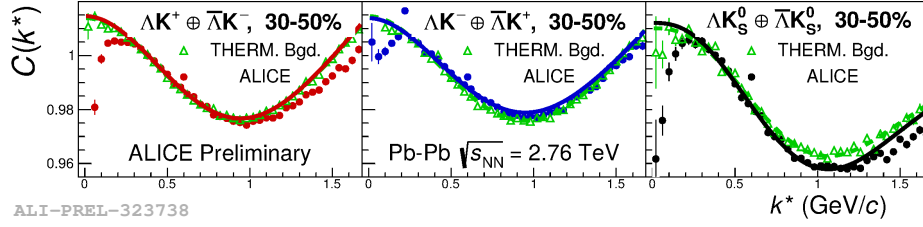
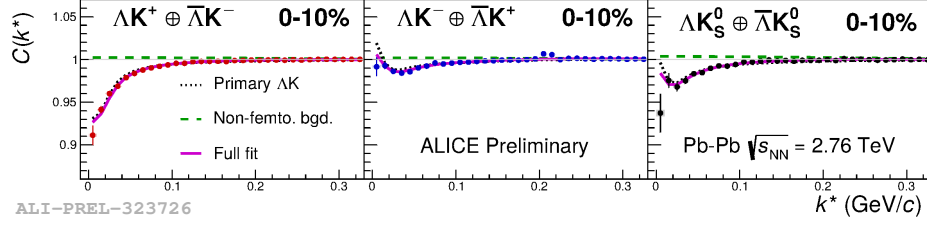


**Fig. 1.** THERMINATOR 2 simulation (open triangles) with experimental data (closed circles) for the 30–50% centrality range. Results are shown for  $\Lambda K^+$  (left),  $\Lambda K^-$  (middle), and  $\Lambda K_S^0$  (right). A 6<sup>th</sup>-order polynomial fit to the simulation is shown as a dashed curve. This polynomial scaled to match the experimental data is drawn as a solid curve.

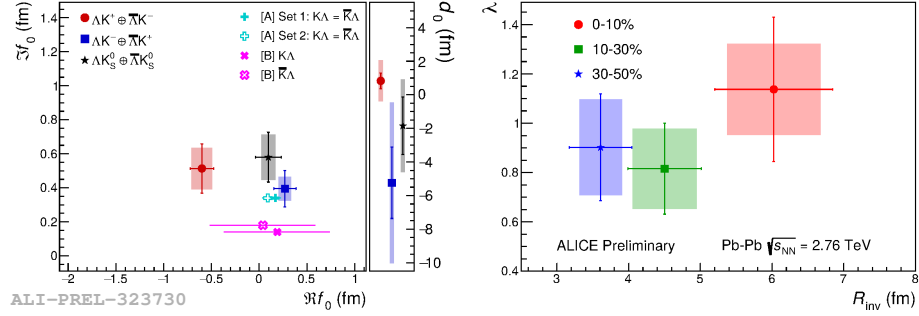
## 4 Results

Figure 2 shows experimental  $\Lambda K$  correlation functions with fits for the 0–10% centrality percentile interval. All six  $\Lambda K$  systems are fit simultaneously across all centralities, with a single radius and  $\lambda_{\text{Fit}}$  parameter for each centrality interval. Scattering parameters ( $\Re f_0$ ,  $\Im f_0$ ,  $d_0$ ) are shared between pair-conjugate systems, but they are assumed unique among the different  $\Lambda K$  charge combinations. Figure 3 summarizes the extracted  $\Lambda K$  fit parameters. For all  $\Lambda K$  systems, positive imaginary parts of the scattering lengths,  $\Im(f_0)$ , describing the inelastic scattering channels, are extracted. More interestingly, the results show that the  $\Lambda K^+$  and  $\Lambda K^-$  systems differ in the sign of the real part,  $\Re(f_0)$ , of their scattering lengths, with a negative value for  $\Lambda K^+$  and positive value for  $\Lambda K^-$  (and  $\Lambda K_S^0$ ). The real part of the scattering length describes the effect of the strong interaction, with a positive value signifying an attraction and a negative value signifying a repulsion. Therefore, the results from this analysis indicate that the

strong force is repulsive in the  $\Lambda K^+$  interaction and attractive in the  $\Lambda K^-$  and  $\Lambda K_S^0$  interactions.



**Fig. 2.** Fit results for the  $\Lambda K$  data in the 0–10% centrality range;  $\Lambda K^+ \oplus \bar{\Lambda} K^-$  are shown in the left column,  $\Lambda K^- \oplus \bar{\Lambda} K^+$  in the middle, and  $\Lambda K_S^0 \oplus \bar{\Lambda} K_S^0$  in the right. The curves show the primary  $\Lambda K$  contribution to the fit, i.e.,  $1 + \lambda_{\Lambda K} C_{\Lambda K}$  in Eq. 2 (dotted), the fit to the non-femtoscopic background (dashed), and final fit (solid).



**Fig. 3.** Extracted fit parameters for all of the  $\Lambda K$  systems. The cross ( $[A] = [8]$ ) and X ( $[B] = [9]$ ) points show theoretical predictions made using chiral perturbation theory.

## 5 Summary

Results from a femtoscopic analysis of  $\Lambda K$  correlations in Pb–Pb collisions at  $\sqrt{s_{NN}} = 2.76$  TeV measured by the ALICE experiment at the LHC have been presented. The femtoscopic radii,  $\lambda$  parameters, and scattering parameters were extracted from one-dimensional correlation functions in terms of the invariant momentum difference. Striking differences are observed in the  $\Lambda K^+$ ,  $\Lambda K^-$ , and  $\Lambda K_S^0$  correlation functions, and the extracted scattering parameters indicate that the strong force is repulsive in the  $\Lambda K^+$  interaction and attractive in the  $\Lambda K^-$  and  $\Lambda K_S^0$  interactions. This effect could be due to different quark–antiquark interactions between the pairs, or from different net strangeness for each system.

## References

1. M.A. Lisa, S. Pratt, R. Soltz, U. Wiedemann, *Ann. Rev. Nucl. Part. Sci.* **55** (2005)
2. G.I. Kopylov, *Phys. Lett.* **B50**, 472 (1974)
3. R. Lednický, V.L. Lyuboshitz, *Sov. J. Nucl. Phys.* **35**, 770 (1982)
4. A. Kiesel, H. Zbroszczyk, M. Szymański, *Phys. Rev.* **C89**(5), 054916 (2014)
5. S. Acharya, et al., *Phys. Rev.* **C99**(2), 024001 (2019)
6. M. Chojnacki, A. Kiesel, W. Florkowski, W. Broniowski, *Comput. Phys. Commun.* **183**, 746 (2012)
7. A. Kiesel, *Acta Physica Polonica B* **48**, 717 (2017)
8. Y.R. Liu, S.L. Zhu, *Phys. Rev.* **D75**, 034003 (2007)
9. M. Mai, P.C. Bruns, B. Kubis, U.G. Meissner, *Phys. Rev.* **D80**, 094006 (2009)